Supporting Information (SI) for "A Selective Dissolution Process Featuring a Classification Device for the Removal of Fines in Crystallization: Experiments"

Pietro Binel and Marco Mazzotti*

Institute of Energy and Process Engineering, ETH Zurich, 8092 Zurich, Switzerland

Email: marco.mazzotti@ipe.mavt.ethz.ch
Phone: +41 44 632 24 56. Fax: +41 44 632 11 41

S1 Sensitivity of the efficiency curve estimate: effect of inaccurate mass measurements

By using the DISCO to measure the suspended mass of crystals, inaccuracies arise due to multiple reasons. In fact, the visual hull volume is an approximation of the true volume of the crystal being observed, and the deviation from the true volume depends on particle size, shape, and orientation in the flow cell. Thus, in general, same amounts of different populations of crystals in suspension will lead to different mass estimates. Further, deviations are expected even when repeating the measurement for the same population, as the third moment of the particle size distribution (PSD) magnifies the statistical noise which is intrinsic to counting devices. The error in the mass estimates, however, has been shown both in the present publication and elsewhere[1] to be rather small, that is within ±6%. To understand to what extent such measurement error affects the estimation accuracy of the efficiency curves, a simulation framework is established.

A feed particle size distribution is generated with a log-normal distribution, whose equation reads

$$n_{\mathrm{f}}(L) = \frac{1}{L\sigma_{\ln}\sqrt{2\pi}} \exp\left(-\frac{(\ln L - \ln \mu_{\ln})^2}{2\sigma_{\ln}^2}\right), \tag{1}$$

where $\mu_{\ln} = 50$ µm and $\sigma_{\ln} = 0.6$ are chosen. We refer to this PSD as the *theoretical* feed PSD, i.e., the PSD of a very large seed population, which can be described with a continuous PSD function. A hypothetical reduced efficiency curve of a hydrocyclone is obtained by using a functional form suggested by Yoshioka and Hotta[2]:

$$E'(L) = 1 - \exp\left[-\left(\frac{L}{d_{50}} - 0.115\right)^3\right] \tag{2}$$

where d_{50} is the cut size and it is close to the inflection point of the function[a]. In our case, d_{50} is set to 50 µm. The efficiency curve is then obtained as

$$E(L) = R_{\mathrm{f}} + (1 - R_{\mathrm{f}})E'(L), \tag{3}$$

[a]One can show that the inflection point is located at $L = 0.115d_{50} + (2/3)^{1/3}d_{50} \approx 0.989d_{50}$. Interestingly, another inflection point is present at $L = 0.115d_{50}$, where the first derivative is also equal to zero. Thus, the functional form by Yoshioka and Hotta should not be used at sizes below $0.115d_{50}$.

where $R_f = 0.20$ is chosen. Given the efficiency curve and the theoretical feed PSD, the theoretical PSDs in the underflow and in the overflow, respectively, are calculated as

$$n_u = E n_f \tag{4}$$

$$n_o = (1 - E) n_f. \tag{5}$$

The three theoretical PSDs are plotted in Figure S1a.

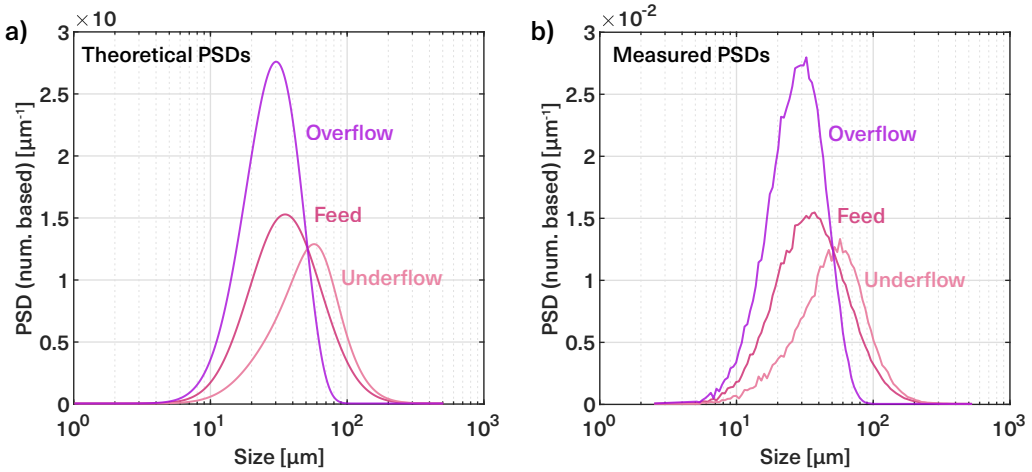

Figure S1: (a) Continuous theoretical PSDs. (b) Simulated measured PSDs.

In a real experiment, however, especially when working at low concentration of suspended particles, the feed population will be discrete and will consist of a finite number of crystals. Thus, an experimental feed PSD is generated by sampling from the theoretical feed PSD a number of particles such that a mass of 0.25 g $\mathrm{kg}_{\mathrm{solvent}}^{-1}$ is reached, thus matching the concentration used in the experiments. The total number of particles sampled, given by the zeroth moment of the distribution, reaches 480,000 per kg of solvent. The experimental PSDs in the underflow and in the overflow are obtained by multiplying the experimental feed PSD by E and $(1 - E)$, respectively, as in Equations (4) and (5).

To simulate the measurement of the experimental feed, underflow, and overflow populations, all have to be sampled from the experimental PSDs. In the underflow, experimentally on average 75,000 particles per kg of solvent are observed over 60 bursts of 500 images collected by each of the two cameras; in the overflow, the figure is about double, i.e., 150,000; in the feed, the sum of the two is assumed. The operation of the DISCO is such that in each burst – lasting about 15 s – the same particle cannot be seen more than once, while this cannot be excluded for different bursts. Thus, the measured PSD is obtained by independently sampling 60 times $N/60$ particles from the experimental PSD, where N is the total number of particles to be sampled. The three measured PSDs, $\hat{n}_f$, $\hat{n}_u$, and $\hat{n}_o$, are plotted in Figure S1b.

Finally, the measured efficiency curve $\hat{E}$ is obtained as

$$\hat{E} = \frac{\hat{n}_u}{\hat{n}_u + \hat{n}_o}, \tag{6}$$

which is to be compared to the theoretical efficiency curve E.

The effect of inaccurate mass measurements is studied by scaling $\hat{n}_u$ and $\hat{n}_o$ in such a way to artificially increase or decrease the mass of crystals in each population. Nine cases are investigated, corresponding to the combination of underestimated, overestimated, and exact mass of both the underflow and the overflow populations. For each case, the biased efficiency curve is calculated for mass

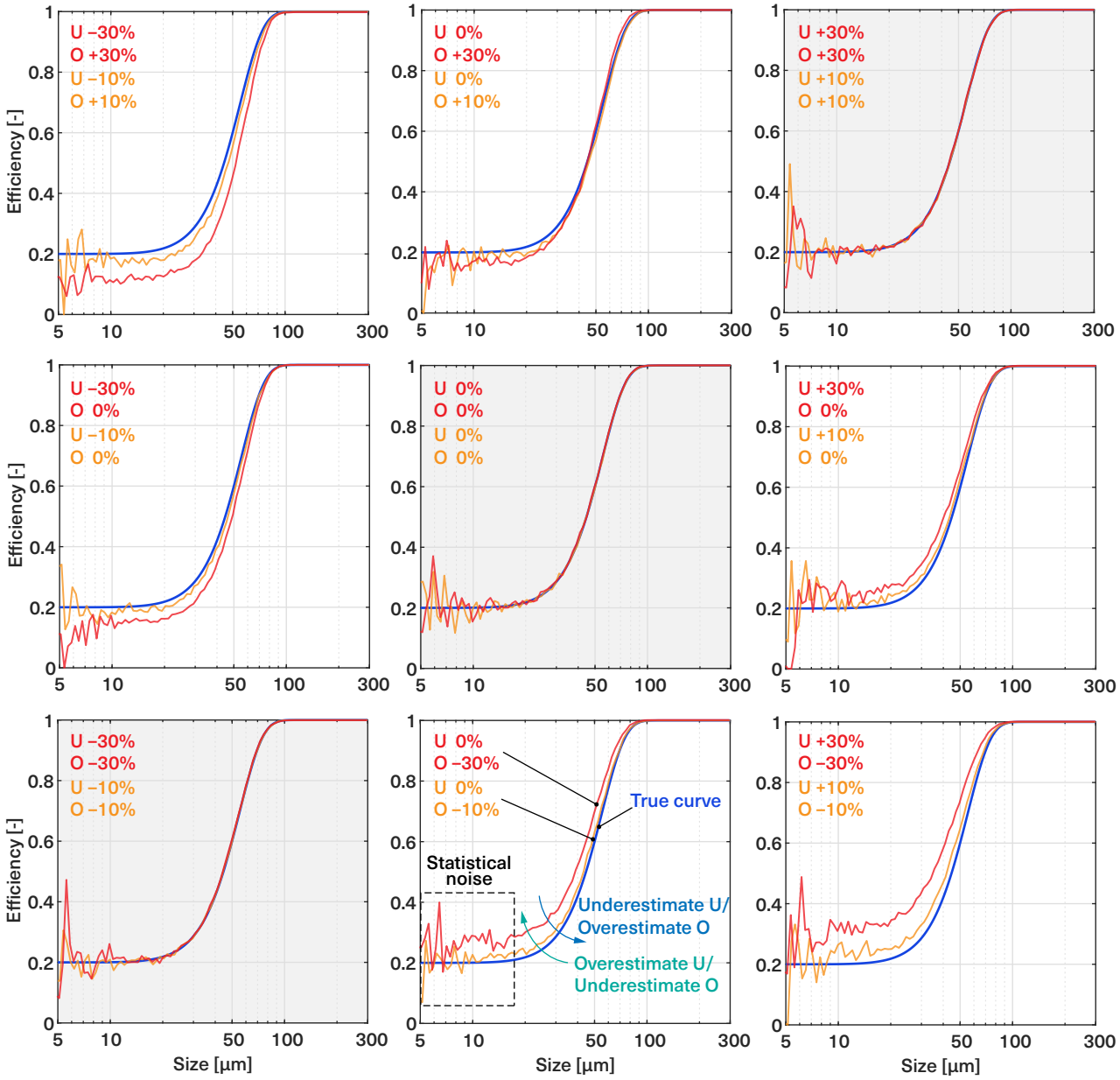

Figure S2: Theoretical efficiency curve (blue line) and simulated measured efficiency curves (red and yellow). Every combination of overestimation and underestimation of the mass of the crystals in the overflow and in the overflow is investigated, considering values of ±10% (yellow) and ±30% (red) with respect to the correct value. In the three plots grayed out on the diagonal, since the mass is measured correctly, or a bias of the same magnitude is introduced for both the underflow and the overflow, the estimate of the efficiency curve is unbiased.

deviations of ±10% and ±30%. The results are shown in Figure S2. The plot in the middle corresponds to the case where the masses of both the underflow and overflow have been estimated correctly; the top right plot and the bottom left plot correspond to the cases in which the masses of the two populations have been both under or overestimated to the same extent. In these three cases the efficiency curve is estimated correctly, since any scaling factor affecting in the same way both populations cancels out in Equation (6).

It can be noted that the curves become noisy below 10 or 20 µm. This is due to the statistical error introduced by sampling from the left tail of the distribution. As a matter of fact, no noise is observed in the right part of the efficiency curve, as $\hat{n}_o$ becomes very small at large sizes irrespective of sampling artifacts, thus making $\hat{E}$ tend to unity.

In general, it is possible to observe that even under extreme circumstances, such as the underestimation of the mass in the underflow by 30% and the overestimation of the mass in the overflow by an equivalent amount (top-left plot), the cut-size of the hydrocyclone is not heavily affected. In fact, the most relevant change in the shape of the efficiency curve is observed in the left tail, which is shifted to a higher or lower value than the R_f. In the specific case of the experimental results presented in the manuscript, where the mass deviation is comprised within ±6%, it can be therefore concluded that no significant error in the estimated efficiency curve is expected.

S2 Pulsation dampener design

A pulsation dampener has been designed and studied with the aim of minimizing the pulsation caused by the peristaltic pump. The device consists of a sealed chamber with one inlet tube and one outlet tube arranged so as to create a siphon. A technical drawing is provided at the end of this document (depicted upside-down compared to the installed orientation). The bottom surface is sloped in such a way that the inlet of the outlet tube is located at the lowest point of the chamber, where any liquid accumulates due to gravity, thus ensuring that the chamber can be completely drained. The device works based on the concept that the air trapped in the chamber acts as a dampener of the fluctuations in inlet flow rate.

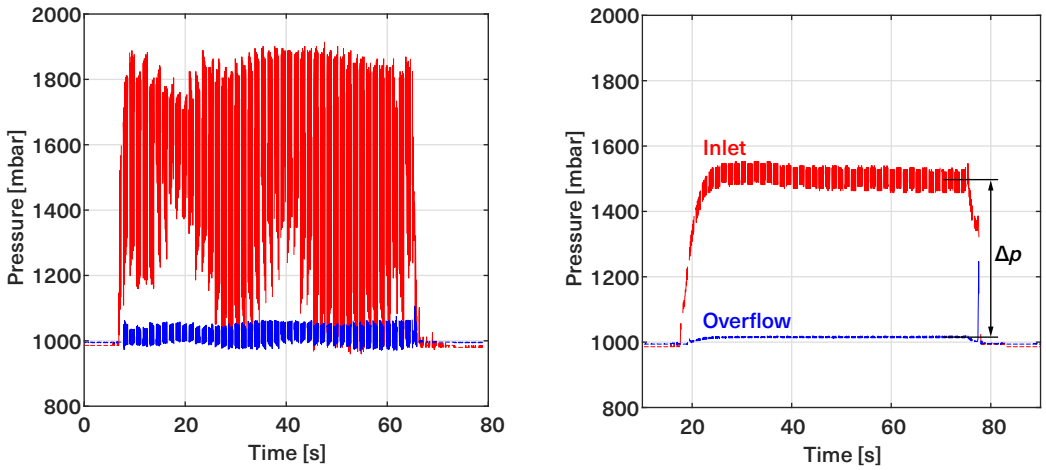

Figure S3: Left: pressure measured without the pulsation dampener. Right: pressure measured with the pulsation dampener.

The benefit of installing such a device becomes evident from Figure S3. While without pulsa-

tion dampener the pressure measured at the inlet of the hydrocyclone fluctuates between 1000 and 1900 mbar, with pulsation dampener the oscillation amplitude is reduced to less than 100 mbar. The pressures at the inlet and at the overflow are calculated by averaging the noisy time-resolved values and the pressure drop is calculated as the difference between the two average values.

S3 Hydrocyclone design

The technical drawing of the hydrocyclone having 21 mm main diameter and 1.50 mm underflow diameter is attached at the end of this document.

S4 Hydrocyclone 3D printing

The top and bottom parts composing the hydrocyclone have been 3D printed with a Prusa i3 MK3S printer. Prusament PETG filament has been selected as a printing material, particularly for its ability of printing steep overhangs, which leads to a good quality of the printed thread. Both a hardened steel and a brass nozzle (0.4 mm) have been tested; the brass nozzle has been found to produce a better surface finish.

The exported CAD models have been sliced with the free software PrusaSlicer 2.3. For the print settings, the default values provided by selecting 0.10 mm layer height and Prusament PETG filament have been employed. The infill has been set to 15% (3D Honeycomb pattern) and 4 perimeters (corresponding to 1.74 mm vertical shell thickness) have been set to ensure a robust final product.

The printing time resulted to be 3 h for the top part and 8 h for the bottom part, including the support material. Support material had to be generated for both parts to provide a stronger anchoring to the smooth polyetherimide (PEI) printing plate. The top part has been printed upside down, i.e., standing on the overflow tube; the bottom part has been printed standing on the underflow surface.

S5 Liquid split ratio: experimental values

The experimental data set collected to estimate the liquid split ratio for both hydrocyclone designs and for different underflow diameters and flow rates is reported in Table S1. For hydrocyclone A, three repetitions are performed for each experiment; for hydrocyclone B, two repetitions. Two values are reported for each experiment: the first number is the mass of water collected in the underflow and the second number is the mass of water collected in the overflow. The mass is expressed in grams.

Table S1: Mass of the underflow and of the overflow measured after the separation to estimate the liquid split ratio

Hydrocyclone A

D_u [mm]	Flow rate F [L min^{-1}]			
	0.95		1.9	
1.5	327.1	1672.2	290.0	1705.0
	331.7	1668.1	292.2	1706.1
	338.1	1660.5	292.6	1705.0
2.0	502.0	1497.3	454.0	1541.5
	502.3	1496.9	451.1	1548.8
	514.4	1484.9	452.4	1544.4
3.0	884.0	1114.2	856.2	1141.8
	925.9	1075.3	844.8	1153.5
	882.1	1117.5	843.4	1154.9

Hydrocyclone B

D_u [mm]	Flow rate F [L min^{-1}]			
	0.95		1.7	
1.6	377.0	1619.8	339.7	1640.8
	374.1	1626.2	343.0	1638.2
2.0	481.8	1515.9	487.3	1510.3
	493.9	1504.1	477.8	1519.7

S6 Performance of the PDP by using the expected mass instead of the estimated mass

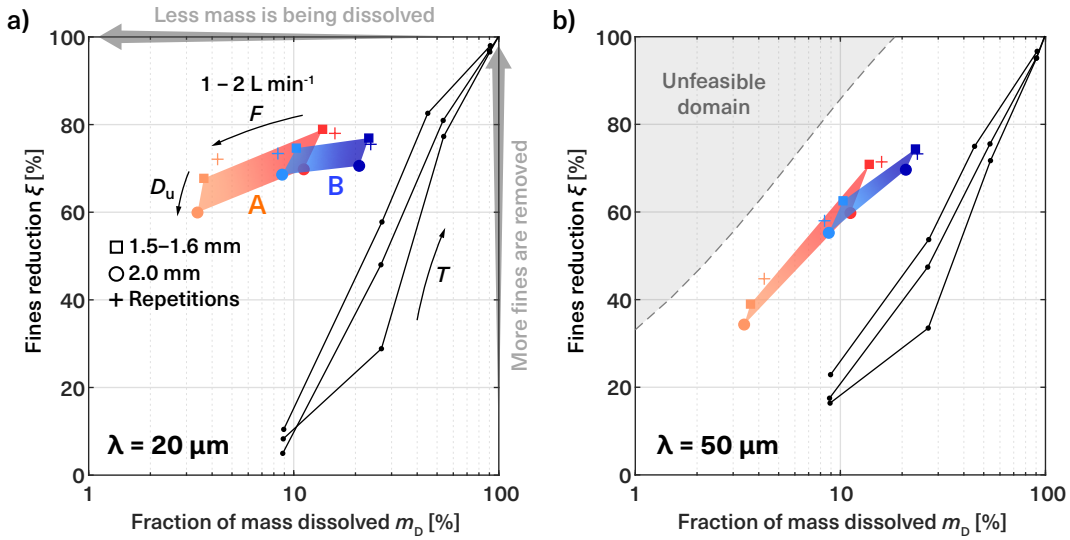

Figure S4: (a) Performance of the SDP (colored regions) and of the PDP (black lines calculated using the expected mass instead of the estimated mass, c.f. Section 4.3) in terms of amount of fines removed ξ per fraction of mass dissolved m_{D}. The value the fines threshold, λ, is 20 µm. For each hydrocyclone design, as in Figure 5, two colors are used for the two flow rates investigated, i.e. in the order of 1 L min^{-1} in the case of red and blue, and 2 L min^{-1} in the case of orange and light blue. Squares are used for $D_{\mathrm{u}} = 1.5 - 1.6$ mm, circles for $D_{\mathrm{u}} = 2.0$ mm, and plus signs represent repetition experiments, to be compared with the squares. (b) Performance of the SDP and of the PDP calculated with the fines threshold $\lambda = 50$ µm. The maximum amount of fines sized up to λ that can be removed for a given fraction of mass dissolved is shown with a dashed gray line; the portion of plane above the line is not reachable and is therefore rendered with a shaded gray fill.

References

[1] Bötschi, S.; Rajagopalan, A. K.; Morari, M.; Mazzotti, M. An Alternative Approach to Estimate Solute Concentration: Exploiting the Information Embedded in the Solid Phase. *The Journal of Physical Chemistry Letters* **2018**, *9*, 4210–4214.

[2] Yoshioka, H.; Hotta, Y. Liquid cyclone as a hydraulic classifier. *Chem. Eng. Jpn.* **1955**, *19*, 632–640.

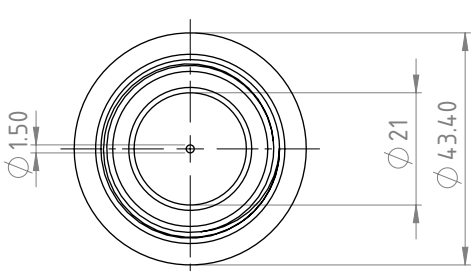

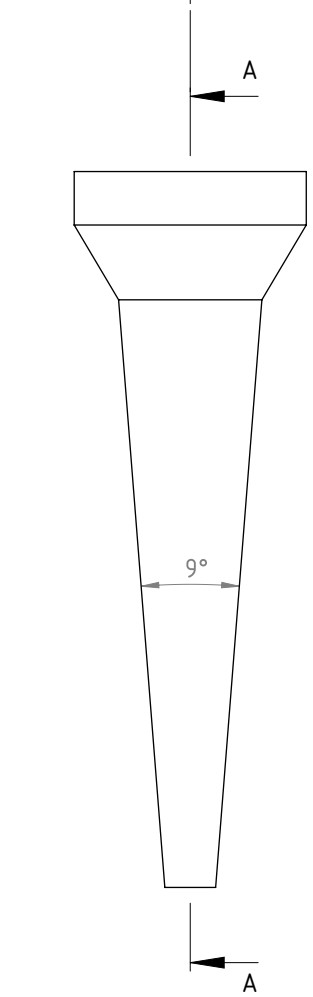

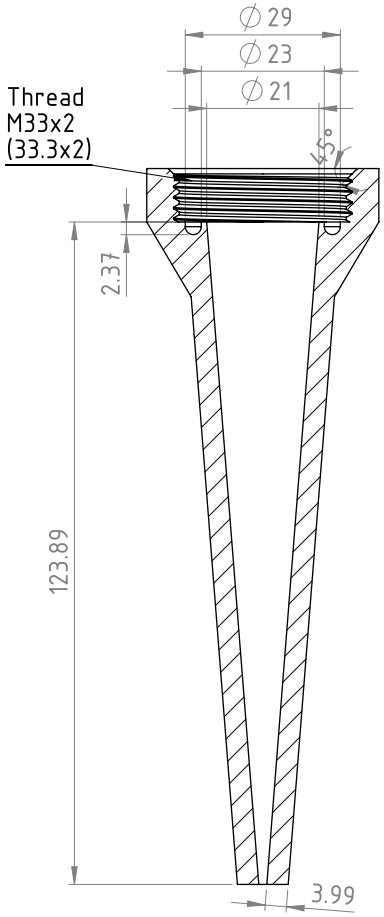

SECTION A-A

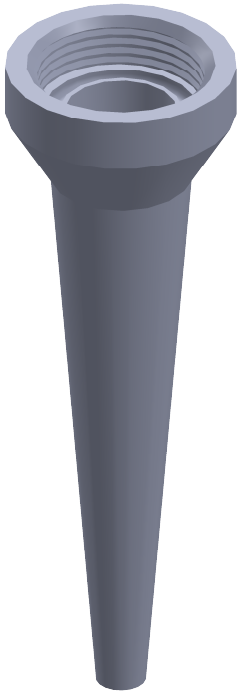

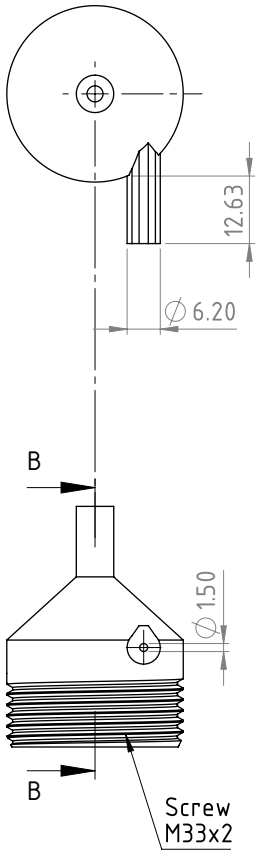

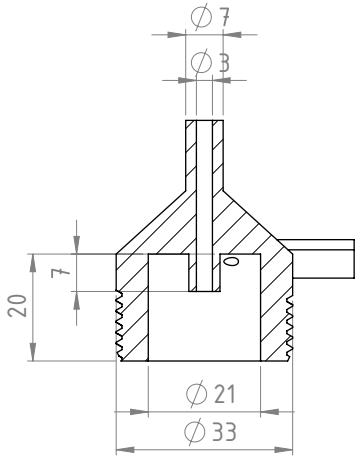

SECTIONB-B

UNLESS OTHERWISE SPECIFIED: DIMENSIONS ARE IN MILLIMETERS SURFACE FINISH: TOLERANCES: LINEAR: ANGULAR:		FINISH:		DEBURR AND BREAK SHARP EDGES		DO NOT SCALE DRAWING	REVISION
	NAME	SIGNATURE	DATE			TITLE: HYDROCYCLONE DESIGN A; D = 21MM	
DRAWN	Pietro Binel		05.04.21				
CHK'D							
APPV'D							
MFG							
Q.A				MATERIAL:		DWG NO.	A3
				WEIGHT:		SCALE:1:1	SHEET 1 OF 1

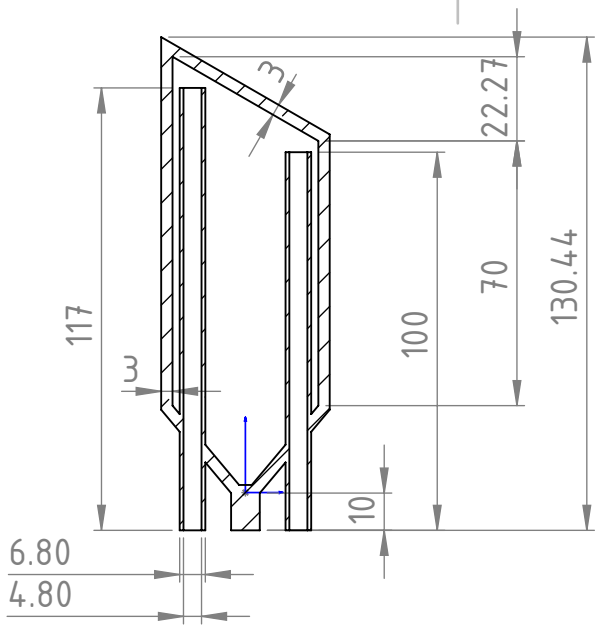

SECTION B-B

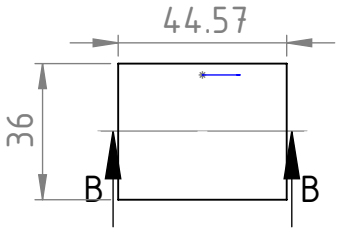

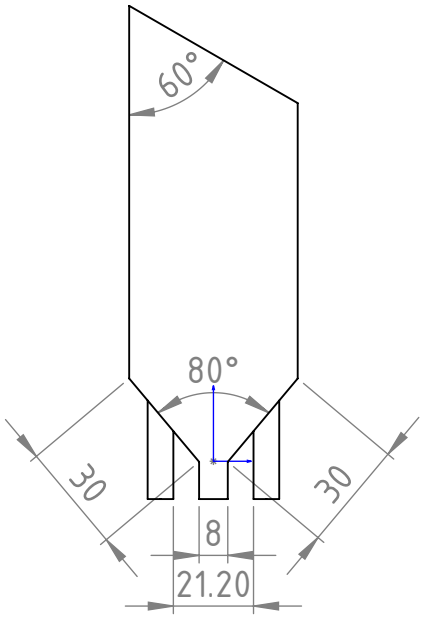

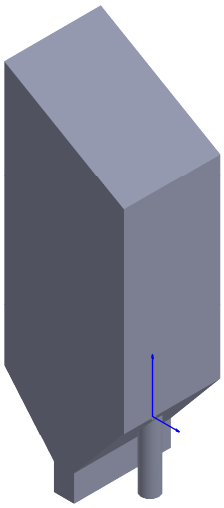

UNLESS OTHERWISE SPECIFIED: DIMENSIONS ARE IN MILLIMETERS SURFACE FINISH: TOLERANCES: LINEAR: ANGULAR:		FINISH:		DEBURR AND BREAK SHARP EDGES		DO NOT SCALE DRAWING	REVISION
	NAME	SIGNATURE	DATE			TITLE:	
DRAWN	Pietro Binel		4.6.21			Pulsation Dampener	
CHK'D							
APPV'D							
MFG							
Q.A				MATERIAL:		DWG NO.	A4
				WEIGHT:		SCALE:1:2	SHEET 1 OF 1